

Southeastern Australian heat waves from a trajectory viewpoint

JULIAN F. QUINTING* AND MICHAEL J. REEDER

School of Earth, Atmosphere and Environment, and ARC Centre of Excellence for Climate System Science, Monash University, Clayton, Australia

ABSTRACT

Although heat waves account for more premature deaths in the Australian region than any other natural disaster, an understanding of their dynamics is still incomplete. The present study identifies the dynamical mechanisms responsible for heat waves in southeastern Australia using 10-day backward trajectories computed from the ERA-Interim reanalyses. Prior to the formation of a heat wave, trajectories located over the South Indian Ocean and over Australia in the lower and middle troposphere ascend diabatically ahead of an upper-level trough and over a baroclinic zone to the south of the continent. These trajectories account for 44% of all trajectories forming the anticyclonic upper-level potential vorticity anomalies that characterize heat waves in the region. At the same time, trajectories located over the South Indian Ocean in the lower part of the troposphere descend and aggregate over the Tasman Sea. This descent is accompanied by a strong adiabatic warming. A key finding is that the temperatures are raised further through diabatic heating in the boundary layer over eastern Australia but not over the inner Australian continent. From eastern Australia, the air parcels are advected southward as they become incorporated into the near-surface anticyclone that defines the heat wave. In contrast to past studies, the importance of cloud-diabatic processes in the evolution of the midlatitude large-scale flow and the role of adiabatic compression in elevating the near-surface temperatures is emphasized. Likewise, the role of the local surface sensible heat fluxes is deemphasized.

1. Introduction

Summer heat waves in Australia have a major effect on many sectors of the community, economy and natural environment. Since the middle of the 19th century, heat waves in Australia have killed more than 5000 people, making these extreme weather situations the deadliest natural hazard of the continent (Coates et al. 2014). And future projections suggest an increase in the intensity, frequency and duration of heat waves in a warmer climate (e.g., Alexander and Arblaster 2009; Cowan et al. 2014), including southeastern Australia. Although statistical investigations of the links between sub-seasonal and seasonal modes of climate variability and southeastern Australian heat waves have received much attention, few studies have focused on the dynamical mechanisms acting on shorter time-scales. Thus, a comprehensive physical picture of how the processes on various time-scales interact is still missing. This picture, however, is an essential part of understanding the mechanisms controlling the location and strength of heat waves, including the changes anticipated in a warmer world.

Numerous studies have investigated how heat waves in southeastern Australia relate to sea surface temperature anomalies and to the dominant intra-seasonal to inter-annual modes of climate variability such as the Southern Annular Mode (SAM; Rogers and van Loon 1982), the Madden-Julian Oscillation (MJO; Madden and Julian 1972), and the El Niño Southern Oscillation (ENSO; Bjerknes 1969). Heat waves in southeastern Australia occur more frequently during episodes of enhanced convection over the Maritime continent and over northern Australia, e.g., during La Niña phases of ENSO, during MJO phases 3–6 of the Wheeler and Hendon (2004)-RMM index, or during active periods of the Australian monsoon (e.g., Parker et al. 2014b; Perkins et al. 2015). During positive phases of SAM, i.e., when the Southern Hemisphere midlatitude jet is shifted poleward, heat waves over southeastern Australia tend to occur more frequently and tend to last longer (Perkins et al. 2015). Although the climate modes provide some information on the amplitude and frequency of southeastern Australian heat waves, the statistical link to climate modes is weaker than for other regions of Australia. Also, southeastern Australian heat waves occur on much shorter timescales than the intra-seasonal to inter-annual modes of climate variability. Thus, processes on shorter synoptic time-scales are expected to be of ma-

* *Corresponding author address:* Julian F. Quinting, School of Earth, Atmosphere and Environment, Monash University, Clayton VIC 3800, Australia.
E-mail: julian.quinting@monash.edu

importance in determining the timing and amplitude of heat waves.

Globally occurring heat waves are typically linked to anomalous anticyclonic flow conditions (e.g., Meehl and Tebaldi 2004; Cassou et al. 2005; Matsueda 2011; Pfahl and Wernli 2012; Stefanon et al. 2012) which can evolve into persistent blocking patterns. Likewise, heat-wave conditions in southeastern Australia are generally associated with tropospheric-deep anticyclonic flow anomalies over the Tasman Sea (e.g., Hudson et al. 2011; Parker et al. 2014a). These anomalies are characterized by positive geopotential height or anticyclonic PV anomalies (i.e., positive anomalies on the Southern Hemisphere) which remain quasi-stationary during the heat wave and roughly centered over the southeast of Australia (e.g., Pezza et al. 2012; Parker et al. 2014a; Purich et al. 2014). The anticyclonic flow anomalies evolve as part of midlatitude Rossby wave packets which have their origin in far upstream regions several days prior to the onset of the heat wave (Parker et al. 2014a). These Rossby wave packets grow in amplitude, start to extend poleward and eventually break anticyclonically over southeastern Australia.

Several dynamical processes have been identified to be conducive to the amplification of the anticyclonic flow anomalies. An investigation of heat waves over southeastern Australia during DJF 1989–2009 reveals the importance of tropical cyclones (TCs) for the intensification of the upper-level anticyclone (Parker et al. 2013). Their analysis suggests that the poleward advection of anticyclonic PV air by diabatically enhanced irrotational flow contributes likely *indirectly* to a poleward extension of the midlatitude anticyclone southeast of the TC. This is in line with recent studies that show the importance of diabatically enhanced irrotational flow for midlatitude flow amplifications on the synoptic time-scale (e.g., Riemer et al. 2008; Archambault et al. 2015; Teubler and Riemer 2015; Quinting and Jones 2016; Grams and Archambault 2016; Bosart et al. 2017).

In addition, the *direct* injection of diabatically processed anticyclonic PV air from the upper-level TC outflow contributes to a further strengthening of the upper-level anticyclone (e.g., Parker et al. 2013; Grams et al. 2011; Grams and Archambault 2016). Likewise, the *direct* injection of diabatically processed anticyclonic PV air from midlatitudes could enhance the anticyclone. In midlatitudes, the *direct* diabatic PV modifications occurring on synoptic time-scales are usually associated with rapidly ascending and coherent air streams, so-called warm conveyor belts (WCBs; e.g., Harrold 1973; Carlson 1980). Diabatic processes during the WCB ascent lead to a net cross-isentropic transport of low-PV air into regions that are climatologically located in the lower stratosphere (Madonna et al. 2014), producing intense anticyclonic PV anomalies. Although several studies in midlatitude dynamics have highlighted this process for the formation of

upper-level anticyclones (e.g., Pomroy and Thorpe 2000; Massacand et al. 2001; Croci-Maspoli and Davies 2009; Grams et al. 2011), Pfahl et al. (2015) was the first to use a Lagrangian approach to systematically quantify the importance of diabatically processed air masses in the formation of midlatitude blocking anticyclones. Their analysis reveals that diabatically processed air masses are of the same importance for blocking formation as diabatically advected air masses.

It is not yet clear whether the *direct* injection of anticyclonic PV air from the Tropics or midlatitudes is a general feature of southeastern Australian heat waves. In this study, we apply a Lagrangian approach to characterize air masses that are associated with heat waves in southeastern Australia. After introducing the dataset and methodology in Section 2, we analyze in Section 3 the characteristics of the air masses of which upper-level anticyclones are comprised. Section 3 aims to answer the following questions:

- What is a characteristic pathway of air masses that reach these upper-level anticyclones?
- Is the cross-isentropic transport of anticyclonic PV through diabatic heating important for the formation of heat waves?
- Where does the cross-isentropic transport occur?

Although the analysis in Section 3 helps to explain the dynamics of upper-tropospheric anticyclones during southeastern Australian heat waves, it does not explain the processes that lead to anomalously warm air masses at the surface. Near-surface temperatures during heat waves have been linked to the advection of warm dry air to the affected regions (e.g., Miralles et al. 2014; Perkins 2015), adiabatic warming in sinking air masses (e.g., Black et al. 2004; Galarneau et al. 2012; Pfahl and Wernli 2012; Bieli et al. 2015), and to radiatively driven heating over anomalously dry soils (e.g., Fischer et al. 2007; Quesada et al. 2012; Miralles et al. 2014; Kala et al. 2015; Herold et al. 2016). Concerning the latter process, anomalously dry soils reduce evaporative cooling by latent heat fluxes and increase atmospheric heating due to enhanced sensible heat fluxes. All these processes may co-occur and reinforce each other culminating in mega-heatwaves (Miralles et al. 2014; Fischer 2014) such as the European heat wave of 2003 and the Russian heat wave of 2010. A commonly accepted picture of southeastern Australian heat waves is that the advection of warm and dry air masses from the inner-continent leads to the anomalously high temperatures (e.g., Reeder and Smith 1987; Hudson et al. 2011; Engel et al. 2013; Marshall et al. 2013; Parker et al. 2014a; Bosch et al. 2015; Perkins 2015). Anomalously low antecedent soil moisture also tends to favor the development of heat waves in this region (Mueller and Seneviratne 2012; Perkins et al. 2015; Herold et al. 2016), although

the connection appears to be weaker than in other regions of the world (Perkins et al. 2015). In order to better understand the physical and dynamical processes leading to the anomalously high temperatures that define southeastern Australian heat waves, the pathway of the near-surface air masses is analyzed in Section 4. The analysis addresses the following questions:

- Is there a characteristic pathway of the near-surface air masses?
- How important is adiabatic warming in sinking air masses compared to near-surface diabatic temperature increase in producing heat waves?

The study ends with a concluding discussion in Section 5.

2. Dataset and methodology

All analyses presented in this paper are based on 6-hourly ERA-Interim reanalyses (Dee et al. 2011) on a regular 0.75° latitude–longitude grid. Climatological means in this study always refer to averages over the 30-year period 1981–2010.

a. Definition of southeastern Australian heat waves

The characteristics of trajectories during southeastern Australian heat waves for the period DJF 1989–2009 are investigated. The definition of these heat waves is based on daily maximum and minimum temperatures at 11 weather stations in southeastern Australia (Fig. 1) in the high-quality daily temperature data set (Trewin 2001). Following the definition of Parker et al. (2013), a heat wave is defined as a period of at least three consecutive days for which:

1. the daily maximum temperature for at least one station exceeds the 90th percentile maximum for that station and month;
2. the daily minimum temperature is above the 90th percentile of minimum temperatures for at least two of three days.

This definition yields 32 heat waves in Victoria for the period DJF 1989–2009 with a total of 132 heat wave days. 39 heat wave days fall into December, 36 days into January, and 57 into February. The highest number of heat wave days within a single summer season (15 days) were recorded in 1994–1995 and 1996–1997, respectively. The most prolonged heat wave of 13 days occurred in January–February 2009. Mildura in northwestern Victoria experiences the highest temperatures with the 90th percentile of daily maximum temperature reaching 39.7°C in January (Fig. 1). The 90th percentile of the daily maximum temperature is generally lower in coastal regions than in northern Victoria. However, even in coastal regions the

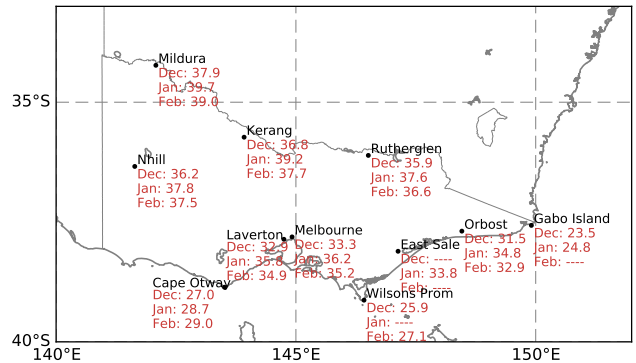


FIG. 1. Map of the 11 weather stations in southeastern Australia that are part of the high-quality daily temperature data set (Trewin 2001). The numbers give the 90th percentile of maximum temperature (in $^\circ\text{C}$) for each station and month. Dashes indicate that a heat wave did not occur at that station and month during 1989–2009. Backward trajectories presented in Section 4 are started from the four ERA-Interim grid points closest to each weather station.

daily maximum temperature can reach 40°C , e.g., Cape Otway on 20 January 1997 (Parker et al. 2014a). For a detailed discussion, the interested reader is referred to Section 3 in Parker et al. (2014a).

b. Definition of anticyclonic upper-tropospheric potential vorticity anomalies

The identification of upper-tropospheric anticyclonic anomalies is motivated by the PV-based atmospheric blocking definition of Schuerz et al. (2004). It is based on the instantaneous 500–150 hPa vertically integrated PV anomaly relative to the monthly climatology of the vertically integrated PV. First, a two-dimensional mask is created that includes all longitude–latitude grid points at which the anomaly of vertically averaged PV is greater than 1 PVU. We then identify all grid points every 50 hPa between 500–150 hPa that lie within the mask. Finally, the instantaneous PV at the identified grid points must be more positive than -1 PVU to exclude grid points in the stratosphere from the analysis. Unlike Schuerz et al. (2004), we are interested in anticyclonic anomalies at all time scales. For this reason the data are not filtered in time, nor is their condition for continuity in time imposed (i.e., their condition that the anomalies calculated in consecutive 6 hour times must at least partially overlap in space). Although the climatological distribution of upper-tropospheric PV anomalies during DJF in the Southern Hemisphere is reasonably uniform in space, they generally occur between 40 to 60°S and on the poleward flank of the 500–150 hPa mean jet (Fig. 2a). Anomalies are climatologically least frequently downstream of South America and to the south of New Zealand.

As outlined in Section 1, southeastern Australian heat waves are characterized by upper-level anticyclonic PV

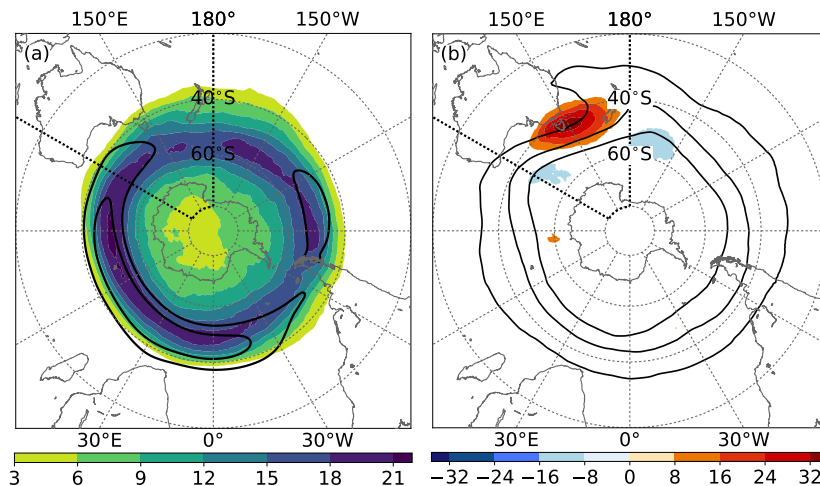


FIG. 2. (a) DJF climatological occurrence frequency of anticyclonic 500–150 hPa PV anomalies (shading in %) and 500–150 hPa mean wind speed (contours at 25, 30 m s^{-1}). (b) 500–150 hPa mean PV (contours at 1, 2, 3 PVU) and anomalous occurrence frequency of 500–150 hPa anticyclonic PV anomalies during southeastern Australian heat waves (shading in %).

anomalies that evolve as part of a midlatitude Rossby wave packet (Parker et al. 2013; Parker et al. 2014a). Composites of vertically averaged PV for all heat wave days corroborate these findings. The vertically averaged PV reveals a midlatitude trough along 120°E (black contours in Fig. 2b) and a downstream ridge that breaks anticyclonically as indicated by the overturning 1 PVU contour. The upper-level ridge is collocated with a positive anomalous occurrence frequency of anticyclonic PV anomalies (shading in Fig. 2b). The location of the occurrence frequency anomaly reveals that the anticyclonic PV anomalies during heat waves occur farther equatorward compared to climatology (cf. shading in Figs. 2a, b).

c. Trajectory calculations

Two sets of 240-hour (10 days) backward trajectories are computed with the Lagrangian analysis tool (LAGRANTO; Sprenger and Wernli 2015) using the ERA-Interim analysis three-dimensional wind field at 60 model levels. Trajectories are started 6-hourly at each day of a heat wave from a regular 0.75° longitude–latitude grid. In order to account for the convergence of meridians towards the poles, all mean quantities presented later in the study are weighted by the square-root of the cosine of the latitude. In this way backward trajectories starting close to the poles are weighted less than trajectories starting farther equatorward when computing statistical quantities of their physical properties. Physical properties that are traced along the trajectories include specific humidity, PV, potential temperature, temperature, anomalies of PV relative to the monthly climatology, cloud liquid water content, and cloud ice water content. Changes in potential temperature between two times along the trajectory are attributed to

adiabatic processes. Although PV is conserved in the absence of diabatic processes, the PV anomalies can change along the trajectories as the anomalies are calculated relative to the climatology (an example being the adiabatic advection of high-PV air into regions of climatologically low-PV air).

The first set of trajectories comprises about 3 million trajectories and is designed to document air masses involved in the formation of upper-tropospheric anticyclones. Following the approach of Pfahl et al. (2015), three-dimensional Lagrangian backward trajectories are started from PV anomalies identified in Section 2b between 120°E and the date line, and equatorward of 80°S. We choose this region as anticyclones that are associated with southeastern Australian heat waves typically occur in this longitude range (Fig. 2b). The starting time of the backward trajectories, i.e., the time when the trajectories are located in the upper-tropospheric PV anomalies, is referred to as $t = 0$ h.

The second set comprises about 14,000 trajectories and is designed to analyze the characteristics of air masses close to the surface. These 240-hour backward trajectories are started from the four grid points closest to each of the weather stations that are incorporated in the definition of southeastern Australian heat waves (Fig. 1). We account for variations in the planetary boundary layer height by starting the trajectories 10, 30 and 50 hPa above the surface (Bieli et al. 2015). The starting time of the backward trajectories, i.e., the time when the trajectories are located at the respective weather station, is referred to as $t = 0$ h.

One important limitation in the computation of trajectories from reanalysis data is that the analyzed wind fields do not resolve convection explicitly. This limitation is of particular relevance in the Tropics. Consequently the La-

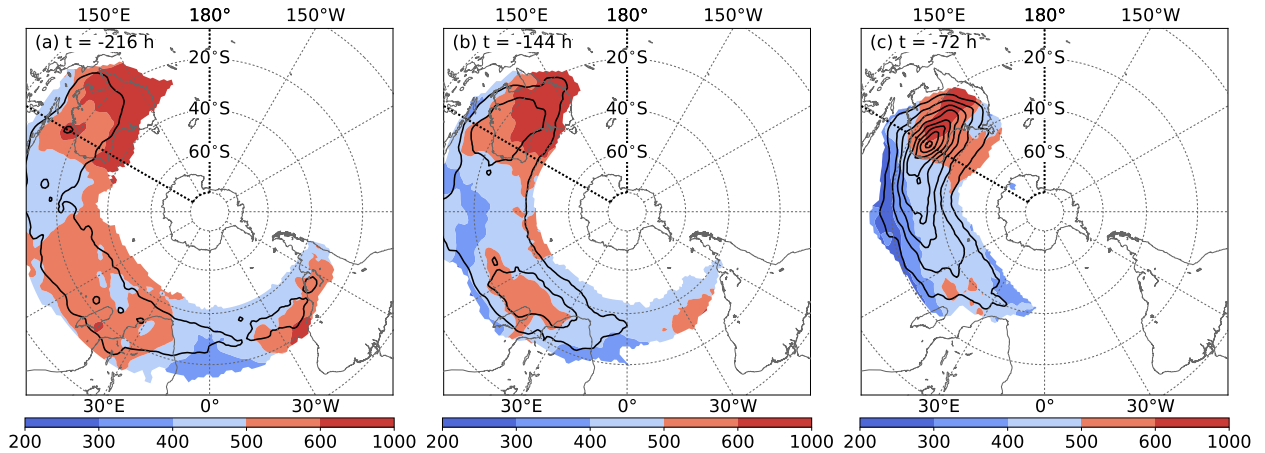


FIG. 3. Mean height (shading in hPa) and spatial density (black contours every $\% 10^{-6} \text{ km}^{-2}$) of trajectories that are involved in the formation of upper-level anticyclones during southeastern Australian heat waves. The times prior to the arrival of the air parcels in anticyclonic anomalies at $t=0\text{h}$ are given in subcaptions.

grangian transports due to sub grid-scale convective cells are not fully represented in the 6-hourly wind fields. In addition, the 6-hourly analysis times might underestimate the vertical displacement of air parcels when convection occurs between two time steps or overestimate the vertical displacement when the vertical motion associated with short-lived convection is applied to the 6-hour period. Nonetheless, case studies and climatological analyses (e.g., Ploeger et al. 2011; Martius and Wernli 2012) indicate that ERA-Interim reanalyses are suitable for trajectory analysis in tropical latitudes.

3. Air masses in upper-tropospheric anticyclones

This section focuses on the history of the air masses defined by the first trajectory set, i.e., those air masses that are located in upper-tropospheric anticyclones over the Australian region at $t=0\text{h}$. Every 6 hours the longitudes and latitudes of all trajectories, their pressure and their 6-hourly potential temperature change are regridded on a regular 1° latitude–longitude grid. The spatial distribution of the trajectories at different times are analyzed from these regridded data. The distributions are normalized by the spatial integral of the trajectory number so that the spatial integral over each distribution yields 100%.

a. Pathway of air masses

At $t=-216\text{h}$, trajectories that end in anticyclonic anomalies during southeastern Australian heat waves (at $t=0\text{h}$) are nearly equally distributed between South America and Australia (black contours in Fig. 3a). Most trajectories are initially located in the subtropics and mid-latitudes. East of South America, South Africa, and over Australia, the trajectories lie on average below 500 hPa (shading in Fig. 3a). Thereafter, these trajectories ascend,

reaching the upper-tropospheric anticyclone, which is located by definition above 500 hPa.

Relatively few trajectories reach the upper-tropospheric anticyclone from tropical latitudes, in particular from the eastern South Indian Ocean and Northern Australia. At $t=-216\text{h}$, the trajectories from the eastern South Indian Ocean between 90 to 110°E are located on average above 500 hPa and consequently do not necessarily ascend to reach the upper-level anticyclone.

At $t=-144\text{h}$, the trajectory densities are highest over the western South Indian Ocean and over the Australian continent (Fig. 3b). The trajectory density in both regions increases from that at $t=-216\text{h}$, indicating a local confluence of the trajectories. Since these trajectories are mostly located in the lower half of the troposphere they must ascend to reach the anticyclone.

Three days prior to reaching the location of the upper-tropospheric anticyclone at $t=0\text{h}$, the density of trajectories over the South Indian Ocean and over the Australian continent increases further as they head towards the PV anomaly (Fig. 3c). The trajectories over the Australian continent are on average located below 500 hPa, and subsequently ascend southward in the final 72 hours to reach the upper-tropospheric anticyclone.

b. Role of diabatic processes

That a large fraction of the trajectories over the Australian continent ascends during the final 72 hours raises the question: how important are diabatic processes for that ascent? In this section, we quantify the proportion of trajectories that are diabatically heated during the three days prior to reaching the upper-tropospheric anticyclone at $t=0\text{h}$ and contrast their evolution with trajectories that are diabatically cooled. To do so, we integrate all 6-hourly changes in the potential temperature along the trajectories

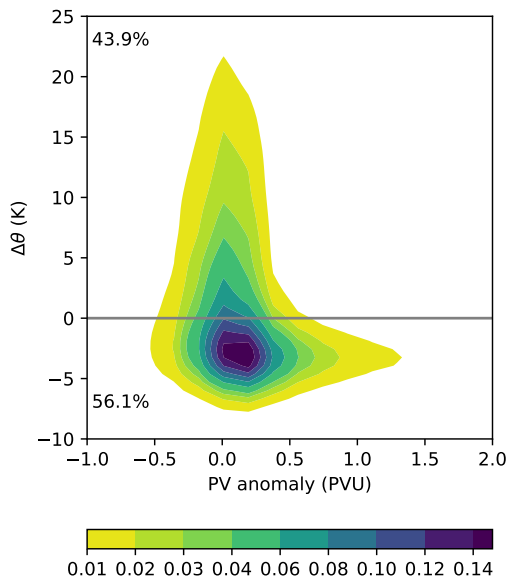


FIG. 4. Joint frequency distribution of PV anomalies at the location of the backward trajectories at $t = -72$ h and integrated change in potential temperature along the trajectories between $t = -72$ h and $t = 0$ h. Shading shows densities of a kernel-density estimate using Gaussian Kernels. We refer to the distribution below (above) the gray line as *horizontal* (*vertical*) branch of the distribution. The numbers give the fraction of trajectories in each branch.

over the three days prior to reaching the location of the anticyclone at $t = 0$ h. This approach follows Pfahl et al. (2015), although they only considered positive potential temperature changes along the trajectories. We find nearly identical results with either approach.

We start by investigating the joint frequency distribution of the integrated potential temperature changes $\Delta\theta$ along the trajectories and of the PV anomaly relative to the monthly climatology at the location of the trajectories at $t = -72$ h. This bivariate joint frequency distribution is obtained by a non-parametric kernel-density estimate using Gaussian kernels (e.g., Wand and Jones 1993).

The distribution of the trajectories involved in the formation of the upper-level anticyclones has two branches (Fig. 4). Hereafter, the term “branch” always refers to the branch of a distribution and not to the branch of an atmospheric air stream. The first branch of the distribution comprises 56% of all trajectories (Table 1, Fig. 4). These trajectories are cooled diabatically between $t = -72$ h and $t = 0$ h, i.e., $\Delta\theta < 0$, while being transported into the upper-level anticyclone. The cooling, which is as much as 8 K in 72 hours, is likely to be radiatively driven. The PV anomalies along this branch range from -0.7 to 1.5 PVU. We refer to this branch as *horizontal* branch. The second branch of the distribution comprises air masses with relatively small PV anomalies, ranging from -0.4 to 0.4 PVU, but with an integrated diabatic heating of up to 22 K. About 44% of the trajectories fall into the second branch (Table 1). We

TABLE 1. Percentage of trajectories in the *horizontal* and *vertical* branches of the distribution relative to the total number of trajectories selected according to their potential temperature θ at $t = 0$ h.

θ at $t = 0$ h	horizontal	vertical
$\theta \geq 350$ K	2%	2%
$\theta < 350$ K	54%	42%
total	56%	44%

refer to this branch of the distribution as *vertical* branch. Although more than half of the trajectories are cooled diabatically between $t = -72$ h and $t = 0$ h, the net effect of all trajectories is a heating due to the strong diabatic heating along the trajectories on the *vertical* branch. Hence, the results show that, as for Northern Hemispheric blocking anticyclones investigated by Pfahl et al. (2015), the transport of diabatically heated air masses is a central part of the formation of anticyclones during southeastern Australian heat waves. As discussed in the next subsection, none of the results are sensitive to the precise definition of the two branches.

In a case study of the Pre-Black Saturday heat wave, Parker et al. (2013) showed that air masses reached the 350-K isentropic level at $t = 0$ h from the Tropics. To determine their pathway systematically, we partition each branch into a set of trajectories that were located below and a set located above the 350-K isentropic level at $t = 0$ h. It is 4% of all trajectories that reach at least 350 K (Table 1). The trajectories above 350 K have their starting points predominantly in the Tropics over Northern Australia and the Maritime Continent (shading in Figs. 5a, d). Most of these trajectories remain confined to this region until $t = -144$ h (shading in Figs. 5b, e), after which they head westward with the climatological upper-tropospheric easterly winds (gray lines in Figs. 6a, f denote height of the trajectories, winds are not shown). At $t = -72$ h, most of the trajectories are located over the central and eastern South Indian Ocean (shading in Figs. 5c, f). From there, they head poleward in the climatologically northerly winds before heading eastward in the midlatitude jet. Overall, the spatial distribution for this set of trajectories is similar for the *horizontal* and *vertical* branches. The described path of the trajectories matches the one in the Pre-Black Saturday heat wave case study by Parker et al. 2013 (their Fig. 2a).

In contrast, trajectories lying on the *vertical* and *horizontal* branches, but not reaching the 350-K isentropic level at $t = 0$ h, reach the anticyclones over Australia along very different pathways. At $t = -216$ h, most trajectories on the *vertical* branch are located in the low- to mid-troposphere (black in Fig. 6a) between South Africa and eastern Australia (red contours in Fig. 5a), whereas those on the *horizontal* branch are located in the mid- to upper-troposphere (black in Fig. 6f) over the South Atlantic and the western South Indian Ocean (red contours in Fig. 5d).

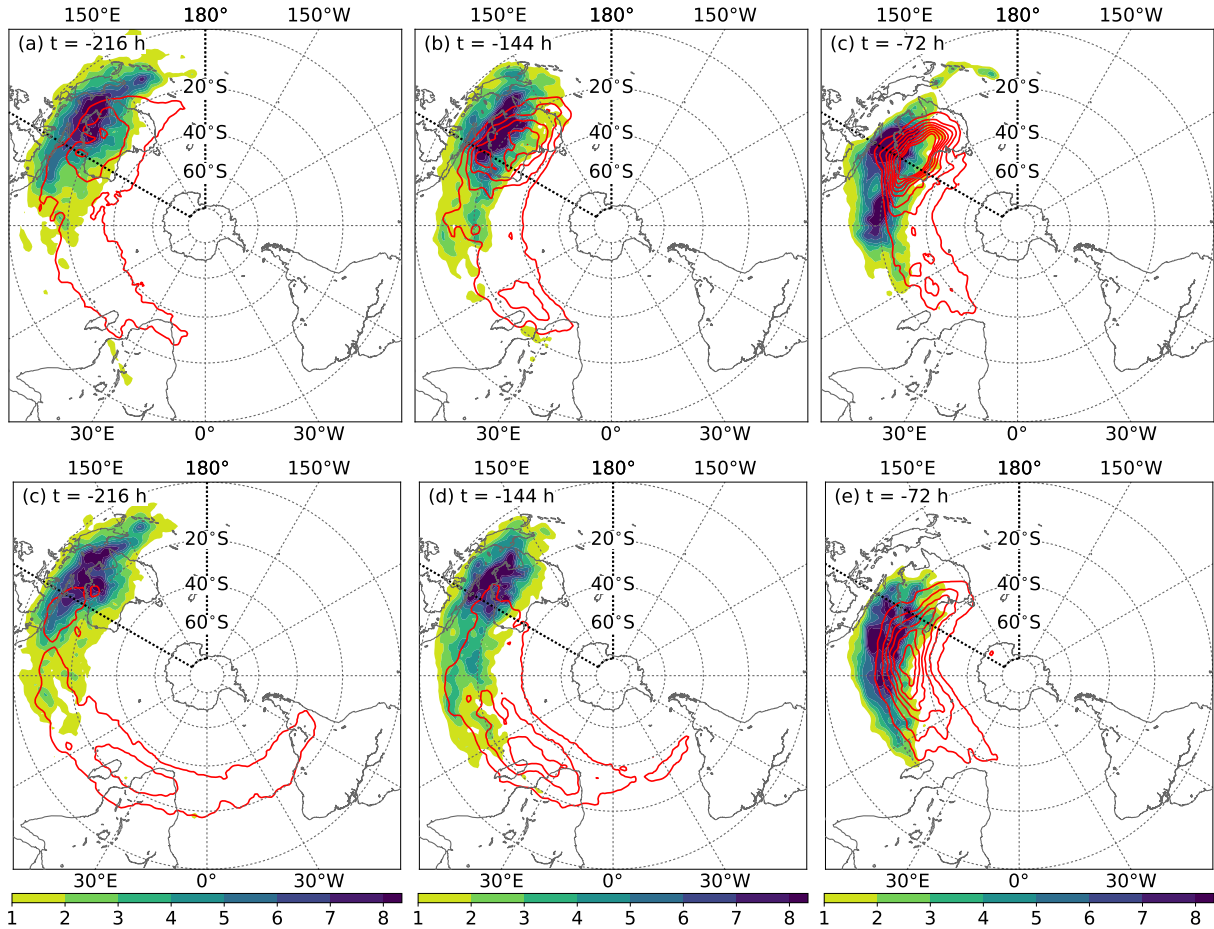


FIG. 5. Spatial densities of trajectories on the *vertical* (top row) and *horizontal* (bottom row) branches at times given in subcaptions. Densities for trajectories above (below) the 350-K isentropic level at $t=0$ h in shading (red contours) every $\% 10^{-6} \text{ km}^{-2}$. The densities are normalized such that the spatial integral yields 100% for each set of trajectories.

The trajectory density on the *vertical* branch is locally highest over the western half of Australia. This local maximum in the trajectory density increases considerably over the next three days such that the largest fraction of the trajectories on the *vertical* branch is located over Australia already 144 hours prior to the arrival in the anticyclone (Fig. 5b). The trajectories on the *horizontal* branch are located between South Africa and Australia too, although the locally highest density occurs over the western South Indian Ocean (Fig. 5e). Though the trajectories on the *horizontal* branch are cooled between $t=-72$ h and $t=0$ h by definition, an additional analysis reveals that between $t=-144$ h to $t=-72$ h a large fraction of these trajectories are actually heated diabatically (not shown). The median trajectory of these diabatically heated trajectories ascends from 700 to 450 hPa, the potential temperature increases by more than 10 K and the specific humidity decreases from 4 to 1 g kg^{-1} . This clearly indicates that the ascent

can at least be partially attributed to cloud diabatic processes over the western South Indian Ocean.

At $t=-72$ h, the spatial distributions of the two branches form a strong dipole over the South Indian Ocean and Australia. Although the trajectories on the *vertical* branch lie mostly over western and central Australia (Fig. 5c), the *horizontal* branch trajectories are mainly located over the South Indian Ocean (Fig. 5f). That the trajectories on the *horizontal* branch are located farther upstream indicates a rapid eastward advection of these air parcels by the mid-latitude jet during the final 72 hours. By definition, the trajectories on the *vertical* branch ascend poleward into the upper-level anticyclone in the next 72 hours (black in Fig. 6a).

In summary, three main trajectory pathways are identified. The trajectories on both branches reaching above the 350-K isentropic level at $t=0$ h are initially located in the upper troposphere of the Tropics. The trajectories on the *vertical* branch that do not reach the 350-K isentropic

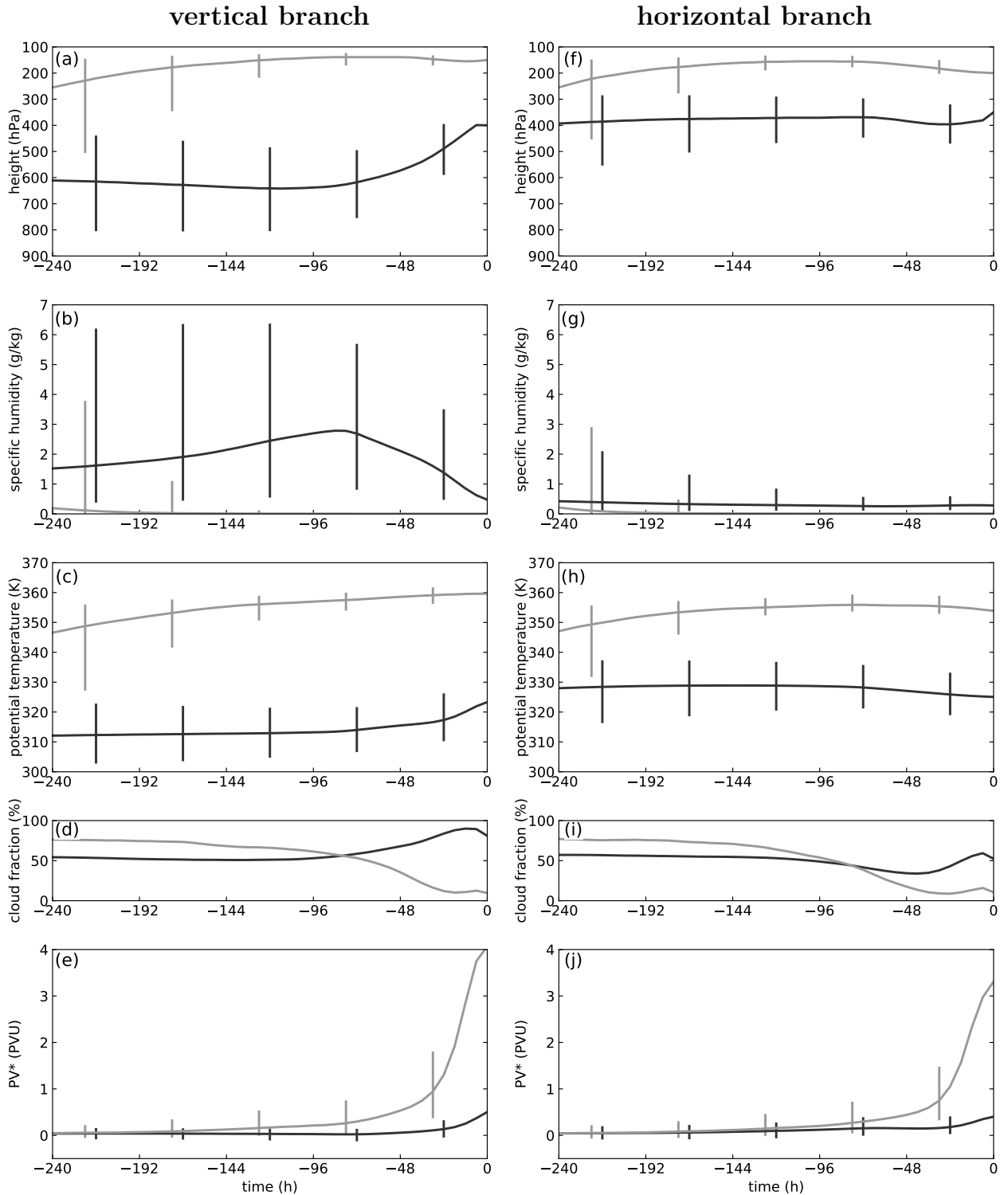


FIG. 6. Temporal evolution of (a, f) height, (b, g) specific humidity, (c, h) potential temperature, (d, i) cloud fraction, and (e, j) PV anomaly along trajectories on the *vertical* (left column) and *horizontal* (right column) branch. Evolution for trajectories above (below) the 350-K isentropic level at $t=0$ h in gray (black). Whiskers give the 25th and 75th percentile, respectively.

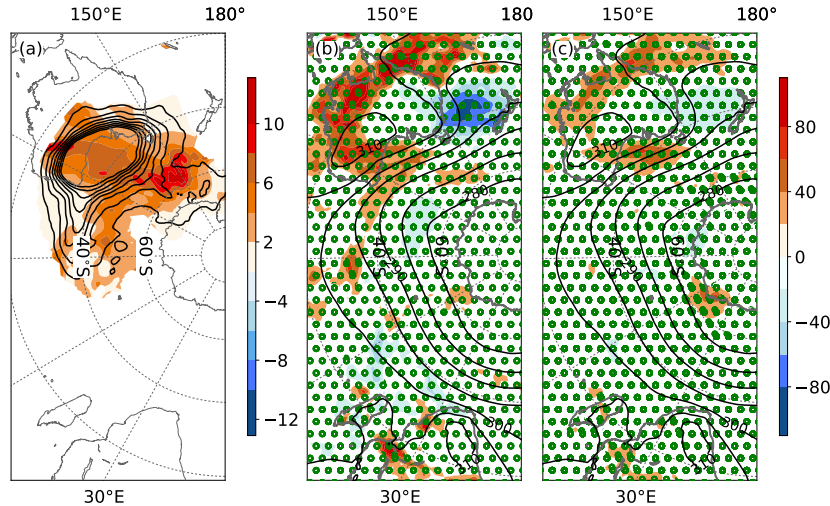


FIG. 7. (a) Spatial density (black contours every $\% 10^{-6} \text{ km}^{-2}$) and mean potential temperature change (K (d)^{-1}) of trajectories on the *vertical* branch at $t = -24 \text{ h}$. Anomalies of (b) cloud liquid and (c) ice water path relative to climatology (shading in g m^{-2}), composite mean of (b) cloud liquid and (c) ice water path (stippled where greater than 100 g m^{-2} and 50 g m^{-2} , respectively, and (b, c) 850-hPa potential temperature (black contours every 5 K) at $t = -24 \text{ h}$.

level start in the lower- to mid-troposphere over Australia and the South Indian Ocean. These trajectories aggregate over the Australian continent before ascending into the upper-level anticyclone. In contrast, the *horizontal* branch comprises trajectories from the mid- to upper-troposphere over the South Atlantic and South Indian Ocean that are advected rapidly eastward with the midlatitude jet.

The differences between the *vertical* and *horizontal* branches are clearly reflected in the physical properties along the trajectories. The trajectories forming the *vertical* branch generally remain in the lower half of the troposphere prior to $t = -72 \text{ h}$ (black in Fig. 6a). About 50% percent of the trajectories are located in the 800–500 hPa layer. The median pressure along the trajectories indicates weak descent from $t = -240 \text{ h}$ to $t = -96 \text{ h}$. This descent, together with the spatial evolution depicted in Figs. 5a–c, suggests that the trajectories mainly descend over the Australian continent before they start ascending into the upper-tropospheric anticyclone. While descending the median specific humidity along the trajectories increases from about 1.5 to 3 g kg^{-1} (black in Fig. 6b), implying that some of the air parcels are moistened by the environment. This moistening occurs mainly along those parcels that are located below 600 hPa (not shown).

That the *vertical* branch trajectories remain in the lower- to mid-troposphere for several days indicates that any forcing mechanisms for ascent are initially missing. During the final 96 hours the median trajectory then ascends from about 600 to 400 hPa (black in Fig. 6a). The ascent is accompanied by a decrease in specific humidity to about 0.5 g kg^{-1} (black in Fig. 6b). The reduction in specific humidity, the simultaneous increase in potential temperature (black in Fig. 6c), and an increase of the

percentage of trajectories inside clouds¹ (black in Fig. 6d) imply diabatic heating through latent heat release. At $t = -48 \text{ h}$, the region of heating is over southern Australia and the Great Australian Bight (Fig. 7a). Composites of the cloud liquid water path and cloud ice water path reveal anomalously high values in the same region (Figs. 7b, c), indicating that the latent heating may be due to both condensation and deposition. A detailed analysis of the cloud microphysical processes is beyond the scope of this study. The region of latent heating as well as the anomalously high cloud liquid- and cloud ice water paths coincide with enhanced rainfall in this region during and before southeastern Australian heat waves as documented in previous studies (see Fig. 6 in Parker et al. 2014a). The forcing for this ascent is potentially provided by an approaching midlatitude trough which typically occurs prior to heat waves over western Australia (black contours in Fig. 2b; Parker et al. 2014a). In addition, the heating occurs along a midlatitude baroclinic zone (black contours in Fig. 7b) indicating slant-wise ascent and highlighting the importance of midlatitude synoptic-scale processes during the evolution of southeastern Australian heat waves.

The trajectories lying on the *horizontal* branch and residing below 350 K start typically at higher levels as indicated by the initially lower pressure (black in Fig. 6f), lower specific humidity (black in Fig. 6g) and higher potential temperature (black in Fig. 6j). Only minor changes in these quantities occur along the trajectories. A slight decrease in potential temperature during the final 96 hours

¹The percentage of trajectories inside clouds is based on the traced cloud ice and liquid water content. Whenever the cloud ice or liquid water content are positive, we assume that the considered air mass is inside clouds.

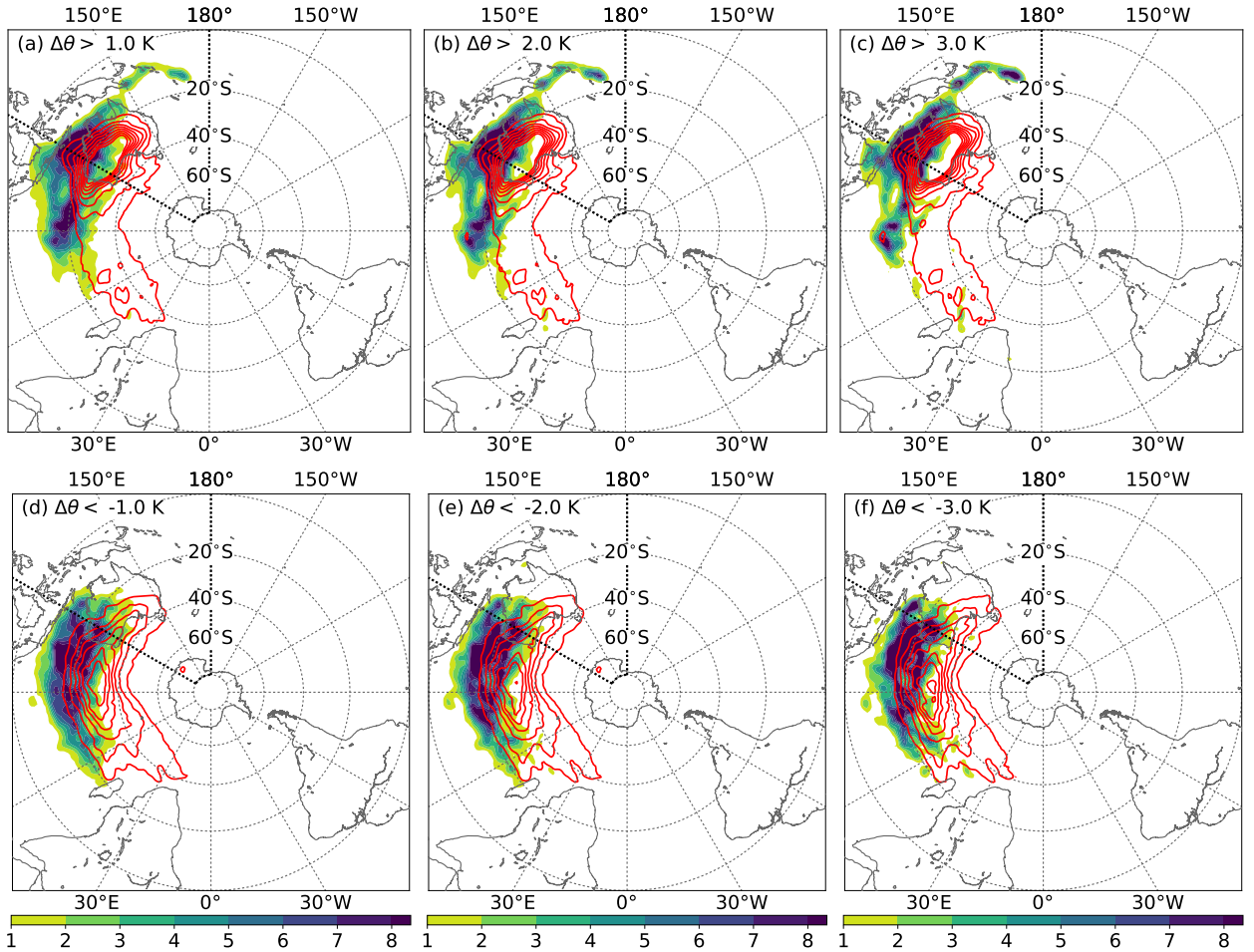


FIG. 8. Spatial densities of trajectories on the *vertical* (top row) and *horizontal* (bottom row) branches at $t = -72$ h for different values of $\Delta\theta$ as given in subcaptions. Densities for trajectories above (below) the 350-K isentropic level at $t = 0$ h in shading (red contours) every $\% 10^{-6} \text{ km}^{-2}$. The densities are normalized such that the spatial integral yields 100% for each set of trajectories.

indicates diabatic cooling accompanied by relatively weak descent. A closer analysis of this potentially radiative cooling is beyond the scope of this study.

The height, specific humidity and potential temperature evolution of the trajectories contributing either to the *vertical* or *horizontal* branch that reach above 350 K are very similar. The majority of trajectories are initially located in the upper-troposphere as shown by an initial median pressure of 250 hPa (gray in Figs. 6a, f). A decrease of the median pressure to 150 hPa before $t = -72$ h is accompanied by a decrease in specific humidity (gray in Figs. 6b, g) and an increase in potential temperature (gray in Figs. 6c, h) indicating diabatic ascent. The trajectories that reach the 350-K isentropic level exhibit a much larger PV anomaly at $t = 0$ h than the rest of the trajectories (Figs. 6e, j). This larger PV anomaly is due to the predominantly adiabatic transport of relatively high-PV air into regions with climatologically much lower PV at this high isentropic level.

c. Sensitivity of results to the definition of the branches

The *horizontal* and *vertical* branches of the joint frequency distribution (Fig. 4) are defined respectively as the subset of trajectories for which $\Delta\theta$ is either negative or positive. Despite the physical association of the two branches with diabatic cooling and diabatic warming, splitting the distribution into two parts along the line $\Delta\theta = 0$ is to some degree arbitrary and leaves open the possibility that the trajectories close to (in some undefined sense) $\Delta\theta = 0$ should belong to a separate adiabatic subset. The sensitivity of the results to this choice is now investigated.

To test the sensitivity, the frequency distribution is partitioned into 3 subsets defined by $\Delta\theta < -\Delta\theta_0$, $-\Delta\theta_0 < \Delta\theta < \Delta\theta_0$ and $\Delta\theta > \Delta\theta_0$, which are the *horizontal*, *adiabatic* and *vertical* branches respectively. $\Delta\theta_0$ is allowed to vary between 0.5 and 3.0 K in 0.5 K increments. For a given $\Delta\theta_0$ the fraction of trajectories in each branch is

TABLE 2. Percentage of trajectories in the *horizontal* and *vertical* branch of the distribution for different values of $\Delta\theta_0$. The *horizontal*, *adiabatic* and *vertical* branches are defined by $\Delta\theta < -\Delta\theta_0$, $-\Delta\theta_0 < \Delta\theta < \Delta\theta_0$ and $\Delta\theta > \Delta\theta_0$.

$\Delta\theta_0$	0.5 K	1.0 K	1.5 K	2.0 K	2.5 K	3.0 K
horizontal	53%	49%	45%	40%	34%	28%
vertical	41%	38%	36%	34%	32%	30%

listed in Table 2. The main point is that, although the fractions of trajectories in the *horizontal* and *vertical* branches decrease with increasing $\Delta\theta$ (as expected), the fractions remain substantial. For example, with $\Delta\theta_0 > 3.0$ K, 30% of the trajectories still lie on the *vertical* branch compared to 43.9% when $\Delta\theta_0 = 0$ K. Moreover, as shown in Fig. 8, the spatial distributions of the trajectories for the *horizontal* and *vertical* branches at $t = -72$ h for three different values of $\Delta\theta_0$ are almost identical to each other and Figs. 5(c, e). Hence, the results reported here are insensitive to the details of how the frequency distribution is divided.

4. Air masses at the surface during heat waves

The Lagrangian analysis presented above shows that the transport of diabatically cooled air masses and cloud-diabatic processes along a baroclinic zone over the Great Australian Bight work in concert during the evolution of the upper-tropospheric anticyclone. A widely accepted paradigm is that the upper-level anticyclone induces a strong low-level northwesterly flow on its western flank which simply advects hot air masses from inner-continental Australia leading to anomalously high temperatures in southeastern Australia. However, there are multiple processes that may contribute to the anomalously high temperatures such as warming through adiabatic descent in the anticyclone or diabatic heating in and above the planetary boundary layer. In order to better understand the processes that lead to anomalously high temperatures at the surface, we analyze the history of the air masses close to the surface and contrast the roles of diabatic and adiabatic processes in producing the anomalously high temperatures. The analysis is based on a set of about 14,000 240-hour backward trajectories starting 10, 30 and 50 hPa above the surface during southeastern Australian heat waves (see Section 2c).

a. Pathway of air masses

The key finding of this analysis is that the hot air masses during southeastern Australian heat waves do not usually originate from the inner Australian continent. Instead, air masses that arrive near the surface during southeastern Australian heat waves are initially located over the South Indian Ocean and the Tasman Sea (black contours in Fig. 9a). At $t = -216$ h, trajectories over the South Indian Ocean lie on average between 700 to 800 hPa (shading in

Fig. 9a). Thus, they must descend by definition to reach the lowest 50 hPa of the troposphere at the time of the heat wave. Likewise, trajectories over the Tasman Sea must descend as they are located between 800 to 900 hPa at $t = -216$ h. The trajectory density increases over the Great Australian Bight and over the Tasman Sea until $t = -144$ h (Fig. 9b). The increase of the average pressure implies descent, particularly over the Tasman Sea where the average pressure increases to more than 900 hPa. At $t = -72$ h, the trajectories are mainly located over the Tasman Sea and over southeastern Australia (Fig. 9c), after which time the trajectories continue to descend over southeastern Australia until $t = 0$ h.

b. Contrasting the role of diabatic and adiabatic processes

Physically, the near-surface air masses can warm either through adiabatic compression as they descend in the anticyclone or diabatically, through sensible, condensational, and radiative heating. In this section, we estimate the diabatic and adiabatic contribution to the temperature change by tracking the potential temperature and temperature along the trajectories.

Air masses that arrive close to the surface during heat waves descend considerably (Fig. 10a). The median pressure increases from about 780 to 940 hPa between $t = -240$ h and $t = -72$ h. This descent warms the air mass adiabatically as indicated by constant potential temperature (Fig. 10b) and an increase in temperature (Fig. 10c). The median temperature along the trajectories increases from 273 to 288 K between $t = -240$ h and $t = -72$ h. The nearly constant potential temperature implies that diabatic processes play a negligible role until $t = -72$ h.

During the final 72 hours, the median temperature along the trajectories increases rapidly to nearly 303 K (Fig. 10c). This temperature increase is mainly due to diabatic processes as indicated by a rapid increase of potential temperature by about 10 K (Fig. 10b). The rapid diabatic heating occurs when the majority of trajectories are no longer over the Tasman Sea, but over southeastern Australia. Composites of ERA-Interim surface sensible heat fluxes reveal that the fluxes are directed upward over the entire continent (i.e., they heat the atmosphere) during the final 48 hours (green contours in Fig. 11a). At $t = -48$ h, the trajectories are located over eastern Australia (black contours in Fig. 11a) in a region of anomalous upward surface sensible heat flux (shading in Fig. 11a), suggesting that the diabatic heating along the trajectories can be linked to upward surface sensible heat fluxes over eastern Australia. The anomalous surface sensible heat flux in that region intensifies until $t = 0$ h (Fig. 11b). It is likely, however, that the increase has only a minor effect on the near-surface trajectories since most of them reach southeastern Australia where the surface sensible heat flux is anomalously low. The region of anomalously low surface

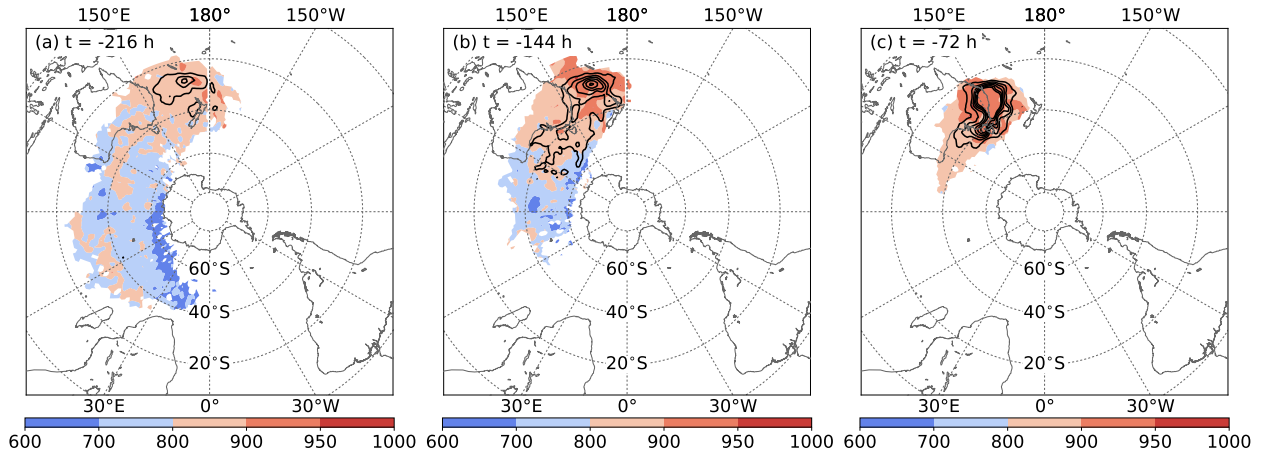


FIG. 9. As in Fig. 3, but for trajectories that arrive close to the surface at $t=0$ h. Note the different color spacing compared to Fig. 3. Contour levels are 4, 8, 12, 16, 20, 24 $\% 10^{-6} \text{ km}^{-2}$.

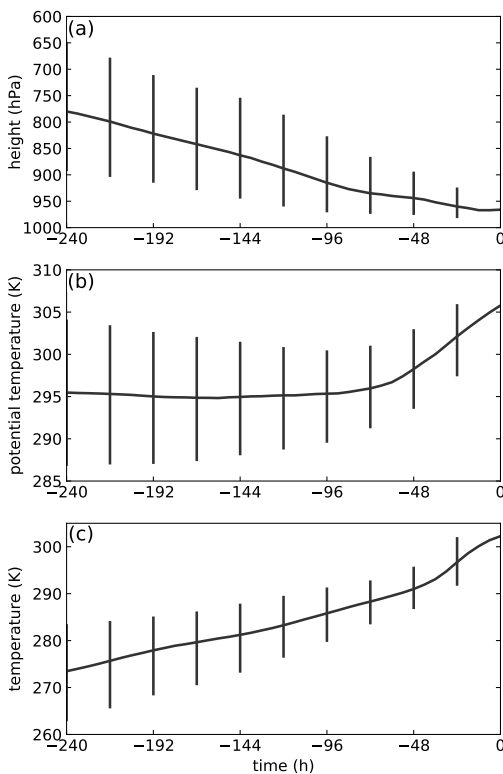


FIG. 10. Temporal evolution of (a) height, (b) potential temperature and (c) temperature along trajectories that arrive close to the surface at $t=0$ h. Whiskers give the 25th and 75th percentile, respectively.

sensible heat flux extends from western Australia toward Tasmania and hence is aligned with the positive anomalies in cloud ice and liquid water content. Presumably the clouds related to the ascent along the baroclinic zone reduce the solar insolation at the surface and weaken the heating of the overlying atmosphere compared to climatol-

ogy. Of course, the net surface sensible heat fluxes are still directed upward leading to a heating of the overlying air mass. Another possibility is that the anomalously low sensible heat fluxes may be due to a lower contrast between the skin temperature and the temperature of the overlying air mass during southeastern Australian heat waves. This possibility is unlikely as the composite difference between skin temperature and the 2-m air temperature during heat waves differs by less than 0.5 K from the climatological mean (not shown).

5. Concluding discussion and outlook

This study is the first to systematically analyze the pathway of air masses involved in 32 southeastern Australian heat waves in the period DJF 1989–2009. First, we analyzed 10-day backward trajectories that ended in upper-tropospheric anticyclones between 120°E to 180° during heat waves.

The analysis identifies the subtropics and midlatitudes between South America to Australia as source regions of air masses 10 days prior to the heat wave. About 44% of all trajectories in the upper-tropospheric anticyclone are heated diabatically during the final 72 hours. These trajectories ascend ahead of an upper-level trough and over a midlatitude baroclinic zone (green contours in Fig. 12) to the south of the Australian continent (label (1) in Fig. 12). This highlights the importance of mid-latitude cloud diabatic processes for the evolution of the upper-level anticyclone. South of Australia and over the South Indian Ocean, trajectories aggregate in the lower-troposphere over several days before they start ascending into the upper-tropospheric anticyclone. This trajectory aggregation is accompanied by weak descent suggesting that air is being circulated in anticyclones over the Indian Ocean and over Australia. The simultaneous increase in specific humidity implies that some of the parcels

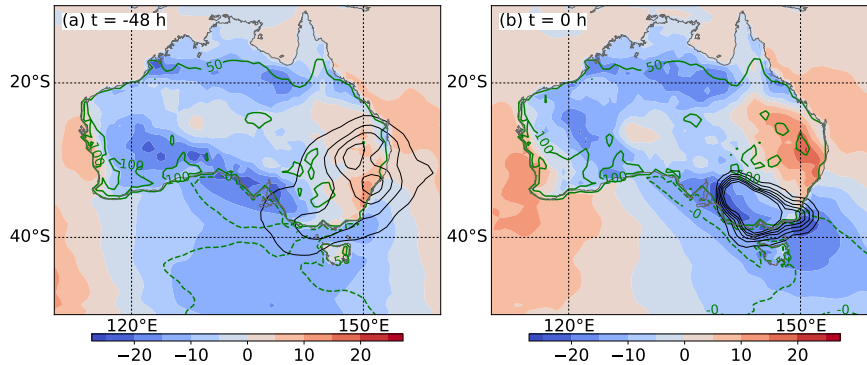


FIG. 11. Spatial density of trajectories that arrive close to the surface at $t=0$ h (black contours at 10, 30, 50, 70, 90, 120 $\% 10^{-6} \text{ km}^{-2}$), anomalies of surface sensible heat flux (shading in W m^{-2}), and average surface sensible heat flux during southeastern Australian heat waves (green contours in W m^{-2}) at times given in subcaptions.

are moistened by the environment. This moistening, primarily along trajectories in the lower troposphere, indicates shallow convection or surface evaporation as potential sources of moisture. Hence, positive sea surface temperature anomalies or enhanced soil moisture may cause an additional moistening of the air parcels before they ascend diabatically into the upper-level anticyclone during the final 72 hours. Since these trajectories comprise 44% of all trajectories in the upper-level anticyclone the enhanced initial moisture may lead to stronger upper-level anticyclones due to enhanced latent heat release. This would corroborate the findings of Kala et al. (2015) who found that increased soil moisture over the Australian continent lead to a strengthened mid-tropospheric anticyclone over the Great Australian Bight and Tasmania. Interestingly, this stands in contrast to the central European heat wave in 2003 where anomalously dry soils amplified the upper-level anticyclone (Fischer et al. 2007). A future study could use the trajectories of this study to identify regions of moistening and perform sensitivity experiments with changed soil moisture conditions or changed sea surface temperature in the regions of moistening. This physical approach could help to assess the poorly understood causality between regional sea surface temperature anomalies and southeastern Australian heat waves (Purich et al. 2014; Boschat et al. 2016).

That 44% of the trajectories are processed diabatically during the 72 hours prior to reaching the location of the upper-level anticyclone at $t=0$ h corroborates the findings of Pfahl et al. (2015) who found similar results for the formation of atmospheric blocking anticyclones in the Northern Hemisphere. The importance of diabatic processes reveals that climate models with a coarse resolution may not adequately represent the structure of upper-level anticyclones during heat waves. Hence, future studies could investigate the effect of numerical model resolution and the role of convective parameterizations on the representation of the heat waves over Australia.

The remaining 56% of all trajectories are cooled diabatically during the final 72 hours. Although the majority of the trajectories are cooled diabatically between $t=-72$ h and $t=0$ h, the net effect of all trajectories is a heating. This is due to the strong diabatic heating along the trajectories on the *vertical branch*. Prior to being cooled, a large fraction of the trajectories on the *horizontal branch* are actually heated diabatically while ascending over the western South Indian Ocean (label (2) in Fig. 12). This region is climatologically characterized by high frequencies of WCBs (Figs. 4 and 5 in Madonna et al. 2014). Although we do not quantify the fraction of WCB trajectories in our data set, the results suggest that WCBs in remote regions contribute to the formation of upper-level anticyclonic PV anomalies that are then advected with the midlatitude jet (label (3) in Fig. 12) into the anticyclones in the Australian region. Parker et al. (2013) showed this advection of air masses from the western South Indian Ocean into an anticyclone over Australia in a case study of the Pre-Black Saturday heat wave (their Fig. 2a). A detailed analysis of the relation between WCBs over the western South Indian Ocean and Australian heat waves is left for future work. Trajectories that are located above the 350-K isentropic level at $t=0$ h stem from tropical latitudes (label (4) in Fig. 12). These trajectories exhibit the strongest PV anomalies at $t=0$ h, as they end up in regions of climatologically low-PV air.

A widely accepted paradigm is that the upper-level anticyclone induces a strong low-level northerly flow on its western flank which simply advects hot air masses from inner-continental Australia into southeastern Australia. The pathway of these near-surface air masses, i.e., those air masses that actually produce the heat wave is analyzed with a second set of trajectories. The key finding of the near-surface trajectory analysis is that southeastern Australian heat waves do not result from the transport of air masses from the inner-continent into the affected region. This is a marked contrast to the widely-accepted

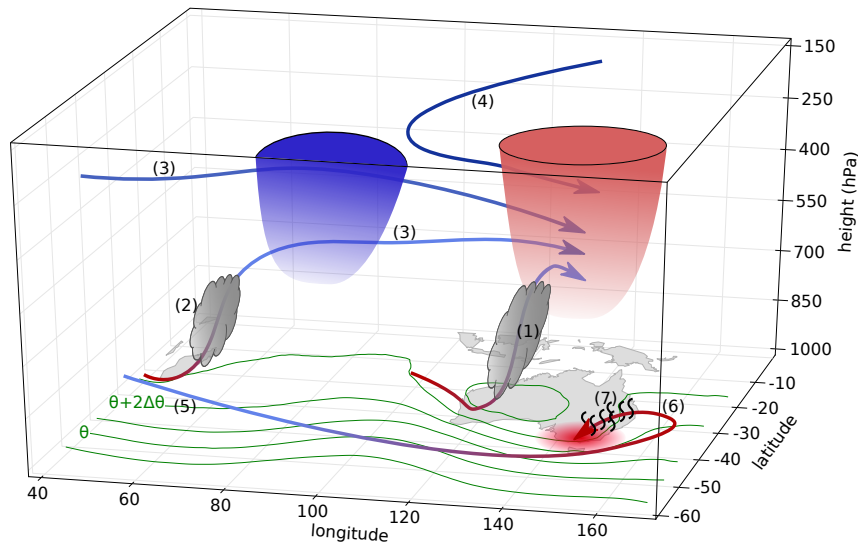


FIG. 12. Sketch of Lagrangian pathways of air masses that are typically involved in the formation of southeastern Australian heat waves. Trajectories are colored by pressure where reddish colors indicate low-levels. Green contours show the low-level potential temperature field and the blue (red) cone denotes upper-level negative (positive) PV anomaly. See Section 5 for details.

view derived from Eulerian fields that low-level northerly winds induced by the upper-level anticyclone simply advect hot inner-continental air to southeastern Australia. Instead, and this is consistent with an analysis of 14 selected heat waves by Bosch et al. (2015), the trajectories reaching southeastern Australia during heat waves are initially located over the midlatitude South Indian Ocean and the Tasman Sea (label (5) in Fig. 12). Until 72 hours prior to the heat wave the trajectories descend adiabatically and aggregate in the anticyclone over the Tasman Sea (label (6) in Fig. 12). The adiabatic descent is associated with a temperature increase of more than 15 K. A large fraction of trajectories that lead to the anomalously high temperatures reach eastern Australia at about $t = -72$ h. Although the spatial distribution of the trajectories during the final 72 hours indicates a northeasterly flow (Fig. 11), the most extreme temperatures still occur in a northwesterly flow which is consistent with previous studies (e.g., Engel et al. 2013; Parker et al. 2014a). For example, 70% of the trajectories during the upper-decile heat waves in Melbourne are located northwest of Melbourne at $t = -12$ h (not shown).

The adiabatic warming until $t = -72$ h does not by itself explain the anomalous near-surface temperatures. Once the trajectories reach the Australian continent air parcels are heated diabatically. The temperature along the trajectories increases rapidly by about 10 K in a region of upward directed surface sensible heat fluxes. These are anomalously high over eastern Australia (label (7) in Fig. 12). The anomalous surface sensible heat fluxes may be due to reduced soil moisture which typically reduces evaporative cooling through latent heat fluxes and

increases atmospheric heating from sensible heat fluxes (e.g., Mueller and Seneviratne 2012). Since the diabatic heating occurs mainly over eastern and southeastern Australia the direct effect of soil moisture conditions on the near-surface air parcels is potentially limited to this region. That low-level diabatic heating increases the likelihood for heat wave conditions corroborates findings of previous studies (e.g., Fischer et al. 2007; Quesada et al. 2012; Miralles et al. 2014; Perkins et al. 2015). However, the combination of anomalously low fluxes in southeastern Australia, and anomalously high fluxes in remote regions indicates that the local soil moisture may not be so important for heat wave conditions. Rather, it may be the transport of air masses heated over anomalously dry soils in remote regions into southeastern Australia that causes the high temperatures. Sensitivity experiments would further elucidate the effect of local and remote soil moisture anomalies on southeastern Australian heat waves. Overall, the analysis of the near-surface trajectories during southeastern Australian heat waves highlights the importance of adiabatic and diabatic processes working in concert to produce anomalously high temperatures.

Although this study sheds light on the dynamics of southeastern Australian heat waves, future studies could investigate how often the identified features exist and a heat wave does not occur. This might be particularly helpful to operational forecasters in southeastern Australia. Also, it would be intriguing to see how the dynamics of extremely hot days that are not part of a heat wave differ from those investigated in this study.

Acknowledgments. JFQ has been supported by the Australian Research Council Centre of Excellence for Climate System Science (CE110001028). We thank Australia's National Computational Infrastructure and ECMWF for providing access to the ERA-Interim reanalysis data. Inspiring discussions with Christian Grams and the helpful comments of three reviewers are gratefully acknowledged.

References

- Alexander, L. V., and J. M. Arblaster, 2009: Assessing trends in observed and modelled climate extremes over Australia in relation to future projections. *Int. J. Climatol.*, **29** (3), 417–435, doi:10.1002/joc.1730.
- Archambault, H. M., L. F. Bosart, D. Keyser, Christopher A. Davis, and J. M. Cordeira, 2015: A composite perspective of the extratropical flow response to recurring western North Pacific tropical cyclones. *Mon. Weather Rev.*, **143** (4), 1122–1141, doi:10.1175/MWR-D-14-00270.1.
- Bieli, M., S. Pfahl, and H. Wernli, 2015: A Lagrangian investigation of hot and cold temperature extremes in Europe. *Q. J. R. Meteorol. Soc.*, **141** (686), 98–108, doi:10.1002/qj.2339.
- Bjerknes, J., 1969: Atmospheric teleconnections from the equatorial Pacific. *Mon. Weather Rev.*, **97** (3), 163–172, doi:10.1175/1520-0493(1969)097<0163:ATFTEP>2.3.CO;2.
- Black, E., M. Blackburn, R. G. Harrison, B. J. Hoskins, and J. Methven, 2004: Factors contributing to the summer 2003 European heatwave. *Weather*, **59** (8), 217–223, doi:10.1256/wea.74.04.
- Bosart, L. F., B. J. Moore, J. M. Cordeira, H. M. Archambault, L. F. Bosart, B. J. Moore, J. M. Cordeira, and H. M. Archambault, 2017: Interactions of North Pacific tropical, midlatitude, and polar disturbances resulting in linked extreme weather events over North America in October 2007. *Mon. Weather Rev.*, **145** (4), 1245–1273, doi:10.1175/MWR-D-16-0230.1.
- Boschat, G., A. Pezza, I. Simmonds, S. Perkins, T. Cowan, and A. Purich, 2015: Large scale and sub-regional connections in the lead up to summer heat wave and extreme rainfall events in eastern Australia. *Clim. Dyn.*, **44** (7), 1823–1840, doi:10.1007/s00382-014-2214-5.
- Boschat, G., I. Simmonds, A. Purich, T. Cowan, and A. B. Pezza, 2016: On the use of composite analyses to form physical hypotheses: an example from heat wave - SST associations. *Nat. Publ. Gr.*, (1), 1–9, doi:10.1038/srep29599.
- Carlson, T. N., 1980: Airflow through midlatitude cyclones and the comma cloud pattern. *Mon. Weather Rev.*, **108** (10), 1498–1509, doi:10.1175/1520-0493(1980)108<1498:ATMCAT>2.0.CO;2.
- Cassou, C., L. Terray, and A. S. Phillips, 2005: Tropical Atlantic influence on European heat waves. *J. Clim.*, **18** (15), 2805–2811, doi:10.1175/JCLI3506.1.
- Coates, L., K. Haynes, J. O'Brien, J. McAnaney, and F. D. De Oliveira, 2014: Exploring 167 years of vulnerability: An examination of extreme heat events in Australia 1844–2010. *Environ. Sci. Policy*, **42**, 33–44, doi:10.1016/j.envsci.2014.05.003.
- Cowan, T., A. Purich, S. Perkins, A. Pezza, G. Boschat, and K. Sadler, 2014: More frequent, longer, and hotter heat waves for Australia in the twenty-first century. *J. Clim.*, **27** (15), 5851–5871, doi:10.1175/JCLI-D-14-00092.1.
- Croci-Maspoli, M., and H. C. Davies, 2009: Key dynamical features of the 2005/06 European winter. *Mon. Weather Rev.*, **137** (2), 664–678, doi:10.1175/2008MWR2533.1.
- Dee, D. P., and Coauthors, 2011: The ERA-Interim reanalysis: Configuration and performance of the data assimilation system. *Q. J. R. Meteorol. Soc.*, **137** (656), 553–597, doi:10.1002/qj.828.
- Engel, C. B., T. P. Lane, M. J. Reeder, and M. Reznay, 2013: The meteorology of Black Saturday. *Q. J. R. Meteorol. Soc.*, **139** (672), 585–599, doi:10.1002/qj.1986.
- Fischer, E. M., 2014: Climate science: Autopsy of two mega-heatwaves. *Nat. Geosci.*, **7**, doi:10.1038/ngeo2148.
- Fischer, E. M., S. I. Seneviratne, P. L. Vidale, D. Lüthi, and C. Schär, 2007: Soil moisture-atmosphere interactions during the 2003 European summer heat wave. *J. Clim.*, **20** (20), 5081–5099, doi:10.1175/JCLI4288.1.
- Galarneau, T. J., T. M. Hamill, R. M. Dole, and J. Perlwitz, 2012: A multiscale analysis of the extreme weather events over western Russia and northern Pakistan during July 2010. *Mon. Weather Rev.*, **140** (5), 1639–1664, doi:10.1175/MWR-D-11-00191.1.
- Grams, C. M., and H. M. Archambault, 2016: The key role of diabatic outflow in amplifying the midlatitude flow: a representative case study of weather systems surrounding western North Pacific extratropical transition. *Mon. Weather Rev.*, **144** (10), 3847–3869, doi:10.1175/MWR-D-15-0419.1.
- Grams, C. M., and Coauthors, 2011: The key role of diabatic processes in modifying the upper-tropospheric wave guide: A North Atlantic case-study. *Q. J. R. Meteorol. Soc.*, **137** (661), 2174–2193, doi:10.1002/qj.891.
- Harrold, T. W., 1973: Mechanisms influencing the distribution of precipitation within baroclinic disturbances. *Q. J. R. Meteorol. Soc.*, **99** (420), 232–251, doi:10.1002/qj.49709942003.
- Herold, N., J. Kala, and L. V. Alexander, 2016: The influence of soil moisture deficits on Australian heatwaves. *Environ. Res. Lett.*, **11** (6), 1–8, doi:10.1088/1748-9326/11/6/064003.
- Hudson, D., A. G. Marshall, and O. Alves, 2011: Intraseasonal forecasting of the 2009 summer and winter Australian heat waves using POAMA. *Weather Forecast.*, **26** (3), 257–279, doi:10.1175/waf-d-10-05041.1.
- Kala, J., J. P. Evans, and A. J. Pitman, 2015: Influence of antecedent soil moisture conditions on the synoptic meteorology of the Black Saturday bushfire event in southeast Australia. *Q. J. R. Meteorol. Soc.*, **141** (693), 3118–3129, doi:10.1002/qj.2596.
- Madden, R. A., and P. R. Julian, 1972: Description of global-scale circulation cells in the tropics with a 40–50 day period. *J. Atmos. Sci.*, **29** (6), 1109–1123, doi:10.1175/1520-0469(1972)029<1109:DOGSCC>2.0.CO;2.
- Madonna, E., H. Wernli, H. Joos, and O. Martius, 2014: Warm conveyor belts in the ERA-Interim Dataset (1979–2010). Part I: Climatology and potential vorticity evolution. *J. Clim.*, **27** (1), 3–26, doi:10.1175/JCLI-D-12-00720.1.
- Marshall, A. G., D. Hudson, M. C. Wheeler, O. Alves, H. H. Hendon, M. J. Pook, and J. S. Risbey, 2013: Intra-seasonal drivers of

- extreme heat over Australia in observations and POAMA-2. *Clim. Dyn.*, **43** (7), 1–23, doi:10.1007/s00382-013-2016-1.
- Martius, O., and H. Wernli, 2012: A trajectory-based investigation of physical and dynamical processes that govern the temporal evolution of the subtropical jet streams over Africa. *J. Atmos. Sci.*, **69** (5), 1602–1616, doi:10.1175/JAS-D-11-0190.1.
- Massacand, A. C., H. Wernli, and H. C. Davies, 2001: Influence of upstream diabatic heating upon an Alpine event of heavy precipitation. *Mon. Weather Rev.*, **129** (11), 2822–2828, doi:10.1175/1520-0493(2001)129<2822:IOUDHU>2.0.CO;2.
- Matsueda, M., 2011: Predictability of Euro-Russian blocking in summer of 2010. *Geophys. Res. Lett.*, **38** (6), 1–6, doi:10.1029/2010GL046557.
- Meehl, G. A., and C. Tebaldi, 2004: More intense, more frequent, and longer lasting heat waves in the 21st century. *Science*, **305** (5686), 994–997, doi:10.1126/science.1098704.
- Miralles, D. G., A. J. Teuling, and C. C. V. Heerwaarden, 2014: Mega-heatwave temperatures due to combined soil desiccation and atmospheric heat accumulation. *Nat. Geosci.*, **7**, 345–349, doi:10.1038/ngeo2141.
- Mueller, B., and S. I. Seneviratne, 2012: Hot days induced by precipitation deficits at the global scale. *Proc. Natl. Acad. Sci.*, **109** (31), 12 398–12 403, doi:10.1073/pnas.1204330109.
- Parker, T. J., G. J. Berry, and M. J. Reeder, 2013: The influence of tropical cyclones on heat waves in Southeastern Australia. *Geophys. Res. Lett.*, **40** (23), 6264–6270, doi:10.1002/2013GL058257.
- Parker, T. J., G. J. Berry, and M. J. Reeder, 2014a: The structure and evolution of heat waves in Southeastern Australia. *J. Clim.*, **27** (15), 5768–5785, doi:10.1175/JCLI-D-13-00740.1.
- Parker, T. J., G. J. Berry, M. J. Reeder, and N. Nicholls, 2014b: Modes of climate variability and heat waves in Victoria, southeastern Australia. *Geophys. Res. Lett.*, **41** (19), 6926–6934, doi:10.1002/2014GL061736.
- Perkins, S. E., 2015: A review on the scientific understanding of heatwaves—Their measurement, driving mechanisms, and changes at the global scale. *Atmos. Res.*, **164**, 242–267, doi:10.1016/j.atmosres.2015.05.014.
- Perkins, S. E., D. Argüeso, and C. J. White, 2015: Relationships between climate variability, soil moisture, and Australian heatwaves. *J. Geophys. Res. Atmos.*, **120** (16), 8144–8164, doi:10.1002/2015JD023592.
- Pezza, A. B., P. van Rensch, and W. Cai, 2012: Severe heat waves in Southern Australia: Synoptic climatology and large scale connections. *Clim. Dyn.*, **38** (1–2), 209–224, doi:10.1007/s00382-011-1016-2.
- Pfahl, S., C. Schwierz, M. Croci-Maspoli, C. M. Grams, and H. Wernli, 2015: Importance of latent heat release in ascending air streams for atmospheric blocking. *Nat. Geosci.*, **8**, 610–614, doi:10.1038/ngeo2487.
- Pfahl, S., and H. Wernli, 2012: Quantifying the relevance of atmospheric blocking for co-located temperature extremes in the Northern Hemisphere on (sub-)daily time scales. *Geophys. Res. Lett.*, **39** (12), 1–6, doi:10.1029/2012GL052261.
- Ploeger, F., and Coauthors, 2011: Insight from ozone and water vapour on transport in the tropical tropopause layer (TTL). *Atmos. Chem. Phys.*, **11** (1), 407–419, doi:10.5194/acp-11-407-2011.
- Pomroy, H. R., and A. J. Thorpe, 2000: The evolution and dynamical role of reduced upper-tropospheric potential vorticity in intensive observing period one of FASTEX. *Mon. Weather Rev.*, **128**, 1817–1834, doi:10.1175/1520-0493(2000)128<1817:TEADRO>2.0.CO;2.
- Purich, A., T. Cowan, W. Cai, P. van Rensch, P. Uotila, A. Pezza, G. Boschat, and S. Perkins, 2014: Atmospheric and oceanic conditions associated with Southern Australian heat waves: A CMIP5 analysis. *J. Clim.*, **27** (20), 7807–7829, doi:10.1175/JCLI-D-14-00098.1.
- Quesada, B., R. Vautard, P. Yiou, M. Hirschi, and S. I. Seneviratne, 2012: Asymmetric European summer heat predictability from wet and dry southern winters and springs. *Nat. Climate Change*, **2**, 736–741, doi:10.1038/nclimate1536.
- Quinting, J. F., and S. C. Jones, 2016: On the impact of tropical cyclones on Rossby wave packets: A climatological perspective. *Mon. Weather Rev.*, **144** (5), 2021–2048, doi:10.1175/MWR-D-14-00298.1.
- Reeder, M. J., and R. K. Smith, 1987: A study of frontal dynamics with application to the Australian summertime 'cool change'. *J. Atmos. Sci.*, **44** (4), 687–705.
- Riemer, M., S. C. Jones, and C. A. Davis, 2008: The impact of extra-tropical transition on the downstream flow: An idealized modelling study with a straight jet. *Q. J. R. Meteorol. Soc.*, **134** (630), 69–91, doi:10.1002/qj.189.
- Rogers, J. C., and H. van Loon, 1982: Spatial variability of sea level pressure and 500 mb height anomalies over the Southern Hemisphere. *Mon. Weather Rev.*, **110** (10), 1375–1392, doi:10.1175/1520-0493(1982)110<1375:SVOSLP>2.0.CO;2.
- Schwierz, C., M. Croci-Maspoli, and H. C. Davies, 2004: Perspicacious indicators of atmospheric blocking. *Geophys. Res. Lett.*, **31** (6), L06 125, doi:10.1029/2003GL019341.
- Sprenger, M., and H. Wernli, 2015: The LAGRANTO Lagrangian analysis tool – version 2.0. *Geosci. Model Dev.*, **8** (8), 2569–2586, doi:10.5194/gmd-8-2569-2015.
- Stefanon, M., F. D'Andrea, and P. Drobinski, 2012: Heatwave classification over Europe and the Mediterranean region. *Environ. Res. Lett.*, **7** (1), 014 023, doi:10.1088/1748-9326/7/1/014023.
- Teubler, F., and M. Riemer, 2015: Dynamics of Rossby wave packets in a quantitative potential vorticity-potential temperature framework. *J. Atmos. Sci.*, **73** (3), 1063–1081, doi:10.1175/JAS-D-15-0162.1.
- Trewin, B. C., 2001: Extreme temperature events in Australia. Ph.D. thesis, School of Earth Sciences, Univ. of Melbourne, Australia, URL <http://repository.unimelb.edu.au/10187/15879>.
- Wand, M. P., and M. C. Jones, 1993: Comparison of smoothing parameterizations in bivariate kernel density estimation. *Journal of the American Statistical Association*, **88** (422), 520–528.
- Wheeler, M. C., and H. H. Hendon, 2004: An all-season real-time multivariate MJO index: Development of an index for monitoring and prediction. *Mon. Weather Rev.*, **132** (8), 1917–1932, doi:10.1175/1520-0493(2004)132<1917:AARMMI>2.0.CO;2.